Stochastic Gravitational Waves from Early Structure Formation

Nicolas Fernandez,[1] Joshua W. Foster,[2,*] Benjamin Lillard,[3] and Jessie Shelton[2,4]
[1]NHETC, Department of Physics and Astronomy, Rutgers University, Piscataway, New Jersey 08854, USA
[2]Center for Theoretical Physics, Massachusetts Institute of Technology, Cambridge, Massachusetts 02139, USA
[3]Department of Physics, University of Oregon, Eugene, Oregon 97403, USA
[4]Illinois Center for Advanced Studies of the Universe, University of Illinois at Urbana-Champaign, Urbana, Illinois 61801, USA

(Received 12 April 2024; accepted 14 August 2024; published 10 September 2024)

Early matter-dominated eras (EMDEs) are a natural feature arising in many models of the early Universe and can generate a stochastic gravitational wave background (SGWB) during the transition from an EMDE to the radiation-dominated universe required by the time of big bang nucleosynthesis. While there are calculations of the SGWB generated in the linear regime, no detailed study has been made of the nonlinear regime. We perform the first comprehensive calculation of gravitational wave (GW) production in EMDEs that are long enough that density contrasts grow to exceed unity, using a hybrid N-body and lattice simulation to study GW production from both a metastable matter species and the radiation produced in its decay. We find that nonlinearities significantly enhance GW production up to frequencies at least as large as the inverse light-crossing time of the largest halos that form prior to reheating. The resulting SGWB is within future observational reach for curvature perturbations as small as those probed in the cosmic microwave background, depending on the reheating temperature. Out-of-equilibrium dynamics could further boost the induced SGWB, while a fully relativistic gravitational treatment is required to resolve the spectrum at even higher frequencies.

DOI: 10.1103/PhysRevLett.133.111002

Introduction—Cosmologically generated gravitational wave (GW) backgrounds provide a unique opportunity to study the state of the very early Universe at temperatures above big bang nucleosynthesis (BBN) and represent an important new physics target for a number of upcoming and proposed observatories, such as LISA [1,2], DECIGO [3,4], BBO [5], μAres [6], pulsar timing with SKA [7], and others. A notably minimal scenario in which a stochastic GW background (SGWB) may be generated is through structure formation during an early matter-dominated era (EMDE). EMDEs arise in a wide variety of well-motivated contexts [8], making early structure formation a potentially powerful probe of the particle physics of postinflationary reheating [9–24], secluded dark sectors [25–29], and natural axion dark matter models [30–32]. Observationally, an EMDE prior to BBN is consistent with all cosmological observation so long as the return to radiation domination (RD) occurs at a reheating temperature $T_{\rm eq} \gtrsim$ few MeV [33,34].

The growth of scalar perturbations during an EMDE induces stochastic GWs at second order in cosmological perturbation theory; see Ref. [35] for a review. Provided the density contrasts δ remain within the perturbative regime, the induced GW signal can be studied using standard tools from cosmological perturbation theory. This "linear" GW spectrum depends quadratically on the amplitude of the primordial curvature power spectrum $A_{\rm s}$ and is maximized for modes that are horizon size at reheating [36–39]. For this linear GW spectrum to be observable, either the metastable species responsible for realizing the EMDE must undergo faster than exponential decays [39,40] or $A_{\rm s}$ must be significantly enhanced on small scales even in the most optimistic sensitivity scenarios. For marginally detectable $A_{\rm s} \gtrsim 10^{-6}$, this limits the duration of the EMDE to at most seven e-folds of scale factor growth before nonlinear structure forms.

Moreover, it has been suggested that nonlinear dynamics in the large-δ regime may amplify the GW production to more readily observable levels [11]. An accurate calculation of the induced SGWBs produced from nonlinearities during an EMDE is critical in order to accurately characterize the signal associated with this scenario. A recent effort [41] aimed to simulate and quantify the GW production from long EMDEs that realize a nonlinear matter density field prior to decay via an N-body simulation approach. In this Letter, we present work that builds considerably on this first calculation. We perform larger simulations that evolve the metastable decaying matter (DM) species as well as the radiation it produces via decay with fully consistent equations of state and background cosmological evolution. Incorporating the decay radiation (DR) ensures that we capture not only the details of halo formation during the

*Contact author: jwfoster@mit.edu

EMDE but also the subsequent halo evaporation and radiation emission during and after the reheating process. Coupled into our cosmological N-body simulations is a real-time evaluation of the induced tensor perturbations, fully accounting for nonrelativistic matter, relativistic radiation, and scalar potential sources.

Induced tensor perturbations—Tensor perturbations to a Friedmann-Robertson-Walker metric in conformal Newtonian gauge can be numerically evolved by

$$h''_{ij} + 2\mathcal{H}h'_{ij} - \nabla^2 h_{ij} = 4\mathcal{S}^{\mathrm{TT}}_{ij}, \tag{1}$$

where primes indicate differentiation with respect to conformal time, $\mathcal{H}$ is the conformal Hubble parameter, ∇^2 is the Laplacian evaluated with respect to comoving coordinates, and $\mathcal{S}^{\mathrm{TT}}_{ij}$ is the transverse-traceless (TT) component of a source tensor. The source tensor relevant for tensor mode production is given by

$$\mathcal{S}_{ij} = 8\pi G a^2 \mathcal{T}_{ij} - 4\Phi\partial_i\partial_j\Phi - 2\partial_i\Phi\partial_j\Phi, \tag{2}$$

where $\mathcal{T}_{ij}$ is the stress-energy tensor and Φ is the first-order Bardeen potential [42–44]. The TT component can be extracted via spectral projection as developed in [45,46]. A key point here is that our source tensor is composed of quadratic combinations of the scalar potential Φ together with the full nonlinear stress-energy tensor for both radiation and matter species.

Tensor modes are continuously sourced during matter domination, which complicates the identification of the energy density in propagating GWs during the EMDE itself. After the EMDE ends, however, the sources decay and the tensor modes may be taken to be freely propagating, rendering the identification of the final energy density in GWs straightforward [44,47,48].

Simulation framework—To evaluate tensor mode production following Eq. (1), we must evaluate the gravitational dynamics of DM and DR through an EMDE and subsequent transition to RD. We do so using a modified version of the massively parallel code CONCEPT [49]. CONCEPT is capable of both N-body and relativistic fluid dynamics treatments of matter and radiation with nontrivial equation of state [50–53]. We note that CONCEPT performs Newtonian simulations, meaning that the scalar potential propagates instantaneously, unlike our tensor perturbations, which propagate merely at c. As a result, our simulations realize unphysically rapid dynamics at the smallest scales that must be interpreted carefully.

Using custom-generated initial conditions in the conformal Newtonian gauge associated with a long EMDE, we use CONCEPT to evaluate the gravitational evolution of DM as a particle species as it simultaneously decays to produce a DR fluid. We consider an initially scale-invariant spectrum of adiabatic perturbations, and study three different values of the amplitude A_{s} of the curvature power spectrum as described further below. The decay of DM into DR proceeds at a constant rate $\Gamma \sim H_{\mathrm{eq}}$. Perturbative analyses of this system have been done in, e.g., [12,54–56].

The radiation both fully contributes to and experiences the gravitational dynamics of our simulation; we model it by assumption as a perfect fluid. This assumption is in line with the treatment of, e.g., [36–38], and lets us compare directly to the perturbative calculation of Ref. [38] in the linear regime.

Our simulations begin at $a_i \approx 10^{-5}$ in the matter-dominated era, advancing through matter-radiation equality at $a_{\mathrm{eq}} \approx 0.2$ and ending deep in the radiation-dominated era at $a_f \equiv 1$. At a_i, density contrasts are sufficiently small that initial conditions can be generated with the Zel'dovich approximation [57]. Our simulations end late, with a return to RD realized through an adiabatically evolving particle mass for the DM and a self-consistently evaluated background expansion rate, as in [52], together with a real-space treatment inhomogeneously sourcing the DR following the DM distribution, which we have implemented here for the first time. As a result, our simulations capture the effects of not just the collapse of gravitationally bound DM structures as studied in [41], but also the GW emission from the radiation produced in DM decay, which was conjectured to be the dominant source in the nonlinear regime [11]. As an illustration of data evolved by our simulation, we present 2D slice plots of DM densities, DR densities, and the scalar potential in Fig. 1.

Gravitational wave calculation—We calculate GW production in the nonlinear EMD-to-RD scenario in real time as part of our simulations following Eq. (1). Radiation contributions to the source tensor are calculated directly from the fluid grids evolved by CONCEPT. Meshes of the DM energy and momentum densities, which are used to source the DR, and meshes of the DM stress-energy tensor elements, which contribute to the source for tensor perturbations, are generated from particle data using a deconvolved piecewise cubic spline interpolation [58]. Meanwhile, the Bardeen potential is calculated from the total matter and radiation density in the Newtonian approximation, which is sufficient as our initial conditions provide power only to modes that are subhorizon at the decay time when the GW signal is generated.

We perform simulations in a comoving box with periodic boundaries. Fluid dynamics are evaluated with a Kurganov-Tadmor scheme using a second-order forward Runge-Kutta with a Van Leer flux limiter [59]. We evolve Eq. (1) in nondissipative special form [60] using a Störmer-Cowell linear multistep method with a fifth order forward step and sixth order backward step in predict-evaluate-correct-evaluate mode [61]. All spatial differentiations are performed spectrally, and our time step satisfies the Courant-Friedrichs-Lewy condition with $\Delta\tau = \Delta x/20$, where Δx is the comoving lattice scale.

Table I summarizes the simulations considered in this Letter. Our simulations are specified by a box dimension

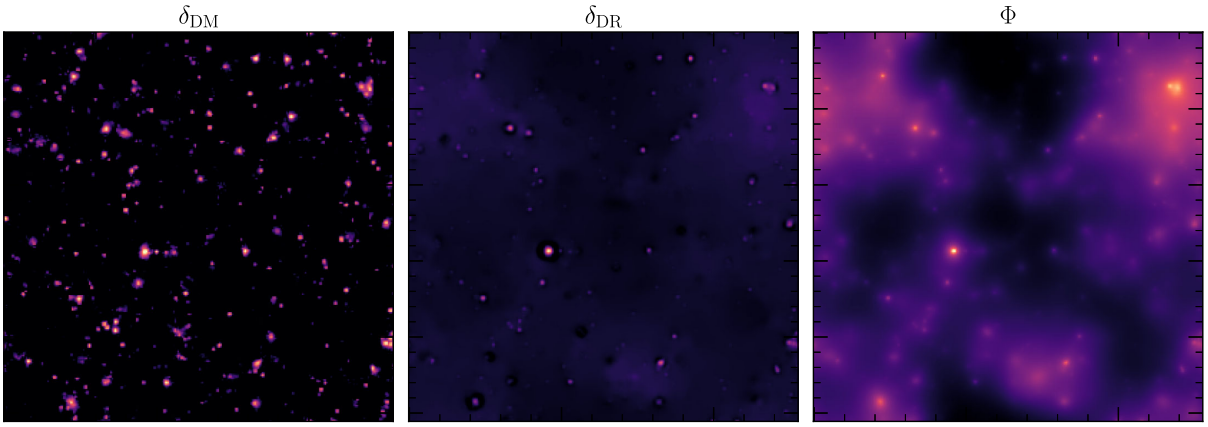

FIG. 1. Left: the density contrast field of DM obtained by meshing particle data at $a_{\rm eq}$ from the $S_{\rm mid}$ simulation. DM clusters, realizing overdensities that have grown as large as $\delta \approx 2300$. Middle: the density contrast field of DR, which does not cluster but traces the spatial distribution of the DM that sources it. In this simulation, we observe overdensities as large as $\delta = 10$. Right: the Newtonian scalar potential produced by the sum of the DM and DR energy densities.

$L_{\rm box}$, a resolution parameter N where N^3 is both the number of lattice sites for GW evolution and the number of particles, and $A_{\rm s}$. We summarize our small-scale resolution in terms of $k_{\rm Nyq}/k_{\rm NL}$, where $k_{\rm Nyq}$ is the Nyquist frequency of the mesh and $k_{\rm NL}$ is the smallest k for which $\Delta_k^2 \geq 1$ at matter-radiation equality. We perform three strongly nonlinear simulations at $A_{\rm s} = 5.4 \times 10^{-5}$, labeled as $\texttt{S}_{\texttt{low}}$, $\texttt{S}_{\texttt{mid}}$, and $\texttt{S}_{\texttt{hi}}$ in terms of their small-scale resolution, and two weakly nonlinear simulations at $A_{\rm s} = 10^{-5}$, labeled $\texttt{W}_{\texttt{low}}$ and $\texttt{W}_{\texttt{mid}}$. We also perform a simulation (Linear) with $A_{\rm s} = 5.4 \times 10^{-13}$, which does not realize any nonlinearity within the simulation resolution and enables comparison with [38]. In Fig. 2, we depict 2D slices of the metric perturbations h_{ij} evaluated from two simulations at $a_{\rm eq}$.

Results—The total GW energy density is calculated by $\rho_{\rm GW} = \langle h'_{ij} h'^{ij} \rangle / (32\pi G a^2)$, with associated energy-density spectrum $\Omega_{\rm GW} = 1/\rho_{\rm c} d\rho_{\rm GW}/d\ln k$. We calculate this spectrum from the late-time field configuration of the tensor perturbations in our simulations. In the left-hand panel of Fig. 2, we present the energy-density spectrum of GWs generated in our strongly nonlinear simulations. We also compare our linear simulation to the perturbative calculation developed in [38], which used approximated fitting formulas that do not capture the full oscillatory behavior of the time-evolving scalar metric perturbations that enter the source for tensor modes. The results of our linear regime simulation demonstrate relatively good agreement with the perturbative calculation in peak height, location, and falloff. In our nonlinear regime simulations, while we do not find significant enhancement of power at the reheat-scale peak, the power at smaller scales is considerably enhanced.

TABLE I. A summary of the six simulations presented in this Letter. We provide the box volume measured in terms of the conformal time at matter-radiation equality, the resolution parameter N, the choice of $A_{\rm s}$ for the scale-invariant initial curvature perturbation, and the small-scale resolution figure of merit $k_{\rm Nyq}/k_{\rm NL}$. See text for details.

Simulation name	$L_{\rm box}/\tau_{\rm eq}$	N	$A_{\rm s}$	$k_{\rm Nyq}/k_{\rm NL}$
Linear	3.84	560^3	5.4×10^{-13}	⋯
$\texttt{S}_{\texttt{low}}$	3.84	560^3	5.4×10^{-5}	11
$\texttt{S}_{\texttt{mid}}$	0.88	256^3	5.4×10^{-5}	22
$\texttt{S}_{\texttt{hi}}$	0.96	560^3	5.4×10^{-5}	44
$\texttt{W}_{\texttt{low}}$	3.84	840^3	1×10^{-5}	11
$\texttt{W}_{\texttt{mid}}$	0.88	384^3	1×10^{-5}	22

One of our main results is that our DR is not an important source of GW emission in the nonlinear regime. This is shown in Fig. 2, where simulations with and without radiation are shown to realize an identical GW spectrum. On linear scales, our results demonstrate that structure formation does not result in substantial enhancement of the GW spectrum over the perturbative prediction. Since we find that the radiation fluid sourced by small-scale nonlinearities is inefficient at transporting anisotropic small-scale power to larger scales, the dominant source for GWs on horizon scales remains the decay of the scalar potentials. Examining Eqs. (1) and (2) reveals that source terms quadratic in Φ have the effect of transferring power across scales down to the horizon scale at reheating, where GW production is efficient. However, in the nonlinear regime, the growth of overdensities slows, leading to a decrease of the scalar potential relative to the linear theory prediction. As a result, matter nonlinearities result in a scale-dependent suppression of scalar potentials and the GWs they produce relative to the linear-theory prediction, which was noted by [36].

On the other hand, we observe significant GW emission at frequencies corresponding to scales that have gone nonlinear. On these scales, the TT source tensor receives its dominant contribution from DM. The collapse into

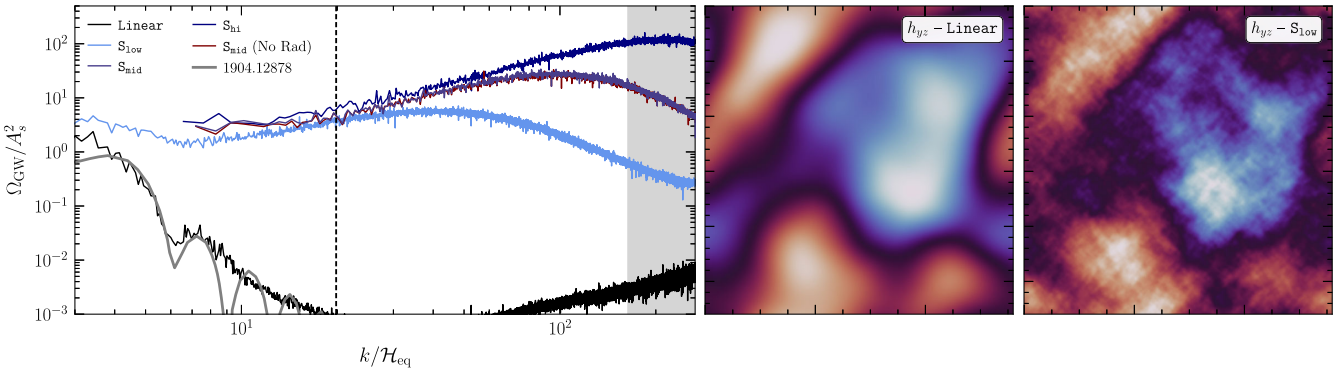

FIG. 2. Left: the spectrum of GW energy density in the Linear simulation and the strongly nonlinear simulation at the three resolution choices considered in this Letter in light, medium, and dark blue in order of ascending small-scale resolution. In red, we show the result from an $\mathtt{S}_{\mathtt{mid}}$ simulation performed without DR, which achieves a GW spectrum identical to that of the $\mathtt{S}_{\mathtt{mid}}$ simulation that includes DR. The dashed black line indicates $k_{\rm NL}$ while the gray band indicates frequencies above the light-crossing time of the largest halos. Right-hand panels: 2D slices of the h_{yz} metric perturbation field evaluated from our Linear and $\mathtt{S}_{\mathtt{low}}$ simulations, which use identical box volume, resolution, and time stepping, differing only in terms of the value of $A_{\rm s}$. Considerably enhanced small-scale structure can be observed in the $\mathtt{S}_{\mathtt{low}}$ simulation, which realizes nonlinear gravitational dynamics within the matter species.

gravitationally bound structures generates anisotropic stress during shell crossing, efficiently sourcing GWs at frequencies associated with the timescales on which DM halos evolve.

The GW emission from collapsing halos is dominated by the largest halos for two reasons. First, the stress energy associated with a halo is given parametrically by $M_h v_h^2$, where M_h is the mass of the halo and $v_h \propto M_h^{1/2}$ the typical speed of its constituents. Second, the largest halos are the latest forming, and so their GW emission is least diluted by redshifting prior to the return to RD, as discussed in [11,41]. Thus the amplitude of the emitted GW spectrum is set by the typical mass scale of halos that are collapsing immediately prior to reheating. Using the Press-Schechter mass function, we can estimate the typical latest-forming halo mass as well as the number density of such halos at reheating in terms of $A_{\rm s}$ and $\mathcal{H}_{\rm eq}$. Assuming a collapsing halo contributes to the GW source tensor in an amount proportional to its total energy, this simple estimate then predicts that the GW energy density sourced by collapsing halos should scale as $\Omega_{\rm GW} \propto A_{\rm s}^{7/4}$, independent of $\mathcal{H}_{\rm eq}$ (see Supplemental Material [62]). We observe exactly this scaling in Fig. 3.

However, the frequency spectrum depends on the dynamical timescale of these halos, which is determined by their density, not their mass. This density is in turn set by the background matter density at the time of formation. Thus the frequency spectrum is determined by the reheating timescale and is independent of the mass scale M_h. This is shown in the left-hand panel of Fig. 3. The cutoff we observe in the small-scale GW power is not physical: as we see from varying N across $\mathtt{S}_{\mathtt{low}}$, $\mathtt{S}_{\mathtt{mid}}$, and $\mathtt{S}_{\mathtt{hi}}$, it comes from the resolution of the simulation.

However, we caution that the Newtonian N-body model allows collapsing halos to act as coherent sources for

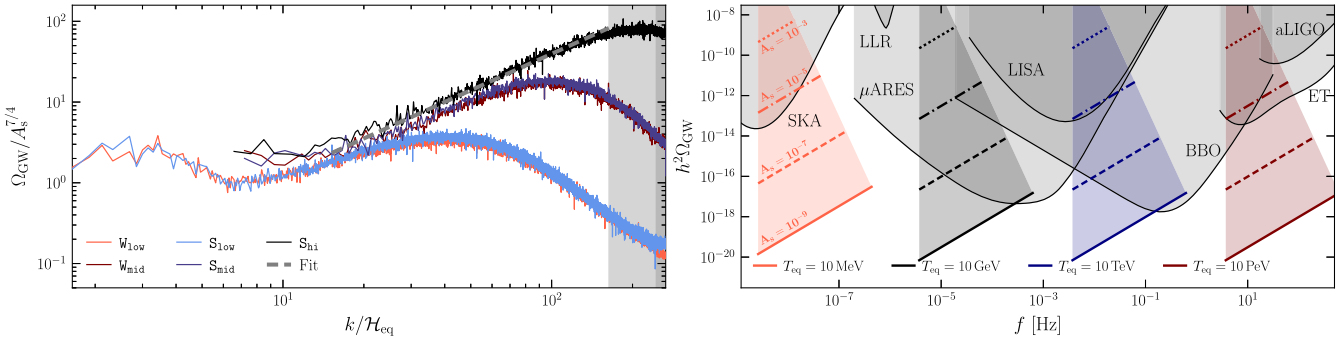

FIG. 3. Left: a comparison of GW spectra between our strongly and weakly nonlinear simulations at equal low and mid resolution of the small-scale dynamics, demonstrating that the morphology of the GW spectrum is independent of $A_{\rm s}$ while its amplitude scales as $A_{\rm s}^{7/4}$. The light (dark) gray band indicates frequencies above the light-crossing time of the largest virialized halos in the strongly (weakly) nonlinear simulations. The dashed gray line shows the fit of Eq. (3). Right: predictions for the induced GW spectrum from Eq. (3) for some representative choices of $T_{\rm eq}$ and $A_{\rm s}$, compared to projected observational sensitivities for future GW observatories obtained from [63–65].

GWs with frequencies substantially above the halo's light-crossing time, and thus for frequencies above the inverse light-crossing time of the largest halos in our simulations, the GW spectrum should be interpreted with care. We expect that, in a more causal treatment, the power radiated by a halo on scales smaller than its light-crossing time would be suppressed by the incoherence of emission across its volume, leading to an M_h and therefore A_s-dependent cutoff.

Comparing to our highest resolution simulation $\mathtt{S_{hi}}$ at k below its resolution cutoff, we find our late-time GW power spectrum to be well approximated by the power-law fit,

$$\Omega_{\mathrm{GW}}(k) \approx 0.05 \times A_s^{7/4} \left(\frac{k}{\mathcal{H}_{\mathrm{eq}}}\right)^{3/2}, \tag{3}$$

with a high-k cutoff at $k_{\mathrm{hi}} \approx 14\mathcal{H}_{\mathrm{eq}}/A_s^{1/4}$ associated with the light-crossing time of the largest virialized halos and a low-k cutoff at $k_{\mathrm{low}} \approx 15\mathcal{H}_{\mathrm{eq}}$, which is of order the collapse time of the latest-collapsing halos. Fitting to $\mathtt{S_{mid}}$ realizes an identical power law index with a $\sim$10% smaller amplitude, consistent with the higher resolution simulation capturing GW production from smaller halos forming at late times. In Fig. 3, right, we compare this spectrum to projected observational sensitivities for several different values of T_{eq} and A_s: depending on the frequency range, we find the SGWB from nonlinear EMDEs is potentially within reach for values of $A_s \gtrsim 10^{-9}$. In the Supplemental Material, we discuss how the dominant role of the largest, latest-collaping structures renders this GW signal insensitive to deviations from scale invariance on much smaller scales [62].

Discussion—Our results provide a conservative and model-independent lower bound on the SGWB resulting from structure formation during an EMDE. The SGWB spectrum that we find reproduces the perturbative prediction on linear scales together with a larger contribution on nonlinear scales, which is dominated by the collapse of the largest and latest-forming halos. We thus expect that, for scale-invariant spectra, the amplitude and location of the nonlinear peak depend on the properties of the EMDE only through T_{eq} and k_{NL}, the largest scale to go nonlinear prior to reheating. Even in our minimal scenario, we find that SGWBs from early structure formation may be within observational reach even for primordial curvature perturbations as small as those probed in the cosmic microwave background (CMB), potentially opening a new window onto the expansion history of the Universe prior to BBN. Intriguingly, a large $A_s \sim 10^{-3}$ initial curvature perturbation spectrum with a low reheat temperature $T_{\mathrm{eq}} \sim 10$ MeV produces a SGWB with amplitude and frequencies broadly similar to the claimed detection by current pulsar arrays [66–69]. However, a more complete characterization of the GW spectrum is required before it is possible to assess the goodness of fit subject to consistency both with primordial black hole constraints [70] and big bang nucleosynthesis [33].

In order to reliably predict the GW spectrum on scales smaller than the light-crossing time of the largest halos, it is necessary to go beyond the framework utilized here and perform a fully relativistic simulation of halo formation, e.g., through the approach of [71]. A more relativistic treatment would also be necessary to make accurate predictions in scenarios of observational interest where the DM decays on a faster-than-Hubble timescale. As a side benefit, such an approach would also correctly handle the difference between Φ and Ψ that is generated by anisotropic stress during the process of collapse, although this effect is subleading.

Finally, we find that as long as the DR can be modeled as a perfect fluid, radiation sourced by the decay of collapsed structures does not provide an important source of GWs. Because anisotropic stress is a leading source for tensor modes, our treatment of the DR as a perfect fluid at equilibrium at all times is a conservative assumption, but one that should be revisited in the future.

Acknowledgments—We particularly thank Jeppe Dakin for guidance regarding working with CONCEPT and feedback on the first version of our manuscript. We thank Malte Buschmann, Patrick Draper, Alan Guth, Misha Ivanov, Toby Opferkuch, Evangelos Sfakianakis, Victoria Tiki, and Helvi Witek for useful conversations. N. F. is supported by the U.S. Department of Energy under Grant No. DE-SC0010008. J. W. F. was supported by a Pappalardo Fellowship. The work of B. L. was supported in part by the U.S. Department of Energy under Grant No. DE-SC0011640. The work of J. S. was supported in part by U.S. DOE Grants No. DE-SC0023365 and No. DE-SC0015655. This work used NCSA Delta CPU at UIUC through allocation PHY230051 from the Advanced Cyberinfrastructure Coordination Ecosystem: Services and Support (ACCESS) program, which is supported by National Science Foundation Grants No. 2138259, No. 2138286, No. 2138307, No. 2137603, and No. 2138296. J. S. gratefully acknowledges MIT's generous hospitality during the performance of this work. This research used resources of the Lawrencium computational cluster provided by the IT Division at the Lawrence Berkeley National Laboratory, both operated under Contract No. DE-AC02-05CH11231.

[1] P. Amaro-Seoane *et al.* (LISA Collaboration), arXiv:1702.00786.
[2] P. Auclair *et al.* (LISA Cosmology Working Group), Living Rev. Relativity **26**, 5 (2023).
[3] S. Kawamura *et al.*, Classical Quantum Gravity **23**, S125 (2006).

[4] S. Kawamura *et al.*, Prog. Theor. Exp. Phys. **2021**, 05A105 (2021).
[5] G. M. Harry, P. Fritschel, D. A. Shaddock, W. Folkner, and E. S. Phinney, Classical Quantum Gravity **23**, 4887 (2006); **23**, 7361(E) (2006).
[6] A. Sesana *et al.*, Exper. Astron. **51**, 1333 (2021).
[7] G. Janssen *et al.*, Proc. Sci., AASKA14 (**2015**) 037 [arXiv: 1501.00127].
[8] R. Allahverdi *et al.*, Open J. Astrophys., 10.21105/astro .2006.16182 (2021).
[9] R. Easther, R. Flauger, and J. B. Gilmore, J. Cosmol. Astropart. Phys. 04 (2011) 027.
[10] K. Jedamzik, M. Lemoine, and J. Martin, J. Cosmol. Astropart. Phys. 09 (2010) 034.
[11] K. Jedamzik, M. Lemoine, and J. Martin, J. Cosmol. Astropart. Phys. 04 (2010) 021.
[12] A. L. Erickcek and K. Sigurdson, Phys. Rev. D **84**, 083503 (2011).
[13] G. Barenboim and J. Rasero, J. High Energy Phys. 04 (2014) 138.
[14] J. J. Fan, O. Özsoy, and S. Watson, Phys. Rev. D **90**, 043536 (2014).
[15] M. A. Amin, M. P. Hertzberg, D. I. Kaiser, and J. Karouby, Int. J. Mod. Phys. D **24**, 1530003 (2014).
[16] M. A. Amin and P. Mocz, Phys. Rev. D **100**, 063507 (2019).
[17] J. Martin, T. Papanikolaou, and V. Vennin, J. Cosmol. Astropart. Phys. 01 (2020) 024.
[18] N. Musoke, S. Hotchkiss, and R. Easther, Phys. Rev. Lett. **124**, 061301 (2020).
[19] J. C. Niemeyer and R. Easther, J. Cosmol. Astropart. Phys. 07 (2020) 030.
[20] B. Eggemeier, J. C. Niemeyer, and R. Easther, Phys. Rev. D **103**, 063525 (2021).
[21] B. Eggemeier, B. Schwabe, J. C. Niemeyer, and R. Easther, Phys. Rev. D **105**, 023516 (2022).
[22] T. Papanikolaou, J. Cosmol. Astropart. Phys. 10 (2022) 089.
[23] K. D. Lozanov and V. Takhistov, Phys. Rev. Lett. **130**, 181002 (2023).
[24] B. Eggemeier, P. Hayman, J. C. Niemeyer, and R. Easther, Phys. Rev. D **109**, 043521 (2024).
[25] Y. Zhang, J. Cosmol. Astropart. Phys. 05 (2015) 008.
[26] C. Blanco, M. S. Delos, A. L. Erickcek, and D. Hooper, Phys. Rev. D **100**, 103010 (2019).
[27] J. A. Dror, E. Kuflik, B. Melcher, and S. Watson, Phys. Rev. D **97**, 063524 (2018).
[28] A. L. Erickcek, P. Ralegankar, and J. Shelton, Phys. Rev. D **103**, 103508 (2021).
[29] A. L. Erickcek, P. Ralegankar, and J. Shelton, J. Cosmol. Astropart. Phys. 01 (2022) 017; 10 (2022) E01.
[30] L. Visinelli and P. Gondolo, Phys. Rev. D **81**, 063508 (2010).
[31] A. E. Nelson and H. Xiao, Phys. Rev. D **98**, 063516 (2018).
[32] N. Blinov, M. J. Dolan, and P. Draper, Phys. Rev. D **101**, 035002 (2020).
[33] P. F. de Salas, M. Lattanzi, G. Mangano, G. Miele, S. Pastor, and O. Pisanti, Phys. Rev. D **92**, 123534 (2015).
[34] T. Hasegawa, N. Hiroshima, K. Kohri, R. S. L. Hansen, T. Tram, and S. Hannestad, J. Cosmol. Astropart. Phys. 12 (2019) 012.
[35] G. Domènech, Universe **7**, 398 (2021).
[36] H. Assadullahi and D. Wands, Phys. Rev. D **79**, 083511 (2009).
[37] K. Kohri and T. Terada, Phys. Rev. D **97**, 123532 (2018).
[38] K. Inomata, K. Kohri, T. Nakama, and T. Terada, J. Cosmol. Astropart. Phys. 10 (2019) 071.
[39] M. Pearce, L. Pearce, G. White, and C. Balázs, J. Cosmol. Astropart. Phys. 06 (2024) 021.
[40] K. Inomata, M. Kawasaki, K. Mukaida, T. Terada, and T. T. Yanagida, Phys. Rev. D **101**, 123533 (2020).
[41] B. Eggemeier, J. C. Niemeyer, K. Jedamzik, and R. Easther, Phys. Rev. D **107**, 043503 (2023).
[42] K. N. Ananda, C. Clarkson, and D. Wands, Phys. Rev. D **75**, 123518 (2007).
[43] D. Baumann, P. J. Steinhardt, K. Takahashi, and K. Ichiki, Phys. Rev. D **76**, 084019 (2007).
[44] A. Ali, Y. Gong, and Y. Lu, Phys. Rev. D **103**, 043516 (2021).
[45] J. Garcia-Bellido, D. G. Figueroa, and A. Sastre, Phys. Rev. D **77**, 043517 (2008).
[46] J. F. Dufaux, A. Bergman, G. N. Felder, L. Kofman, and J.-P. Uzan, Phys. Rev. D **76**, 123517 (2007).
[47] J.-C. Hwang, D. Jeong, and H. Noh, Astrophys. J. **842**, 46 (2017).
[48] G. Domènech and M. Sasaki, Phys. Rev. D **103**, 063531 (2021).
[49] J. Dakin, S. Hannestad, and T. Tram, Mon. Not. R. Astron. Soc. **513**, 991 (2022).
[50] J. Dakin, J. Brandbyge, S. Hannestad, T. Haugbølle, and T. Tram, J. Cosmol. Astropart. Phys. 02 (2019) 052.
[51] T. Tram, J. Brandbyge, J. Dakin, and S. Hannestad, J. Cosmol. Astropart. Phys. 03 (2019) 022.
[52] J. Dakin, S. Hannestad, and T. Tram, J. Cosmol. Astropart. Phys. 06 (2019) 032.
[53] J. Dakin, S. Hannestad, T. Tram, M. Knabenhans, and J. Stadel, J. Cosmol. Astropart. Phys. 08 (2019) 013.
[54] K. Ichiki, M. Oguri, and K. Takahashi, Phys. Rev. Lett. **93**, 071302 (2004).
[55] B. Audren, J. Lesgourgues, G. Mangano, P. D. Serpico, and T. Tram, J. Cosmol. Astropart. Phys. 12 (2014) 028.
[56] V. Poulin, P. D. Serpico, and J. Lesgourgues, J. Cosmol. Astropart. Phys. 08 (2016) 036.
[57] Y. B. Zel'dovich, Astron. Astrophys. **5**, 84 (1970).
[58] E. Sefusatti, M. Crocce, R. Scoccimarro, and H. Couchman, Mon. Not. R. Astron. Soc. **460**, 3624 (2016).
[59] A. Kurganov and E. Tadmor, J. Comput. Phys. **160**, 241 (2000).
[60] D. G. Figueroa, A. Florio, F. Torrenti, and W. Valkenburg, J. Cosmol. Astropart. Phys. 04 (2021) 035.
[61] C. Butcher, Linear multistep methods, in *Numerical Methods for Ordinary Differential Equations* (John Wiley & Sons, Ltd, New York, 2016), Chap. 4, pp. 333–387.
[62] See Supplemental Material at http://link.aps.org/supplemental/10.1103/PhysRevLett.133.111002 for analysis details and additional results that support the conclusions in the main Letter.
[63] P. Campeti, E. Komatsu, D. Poletti, and C. Baccigalupi, J. Cosmol. Astropart. Phys. 01 (2021) 012.
[64] D. Blas and A. C. Jenkins, Phys. Rev. Lett. **128**, 101103 (2022).

[65] D. Blas and A. C. Jenkins, Phys. Rev. D **105**, 064021 (2022).
[66] N. S. Pol *et al.* (NANOGrav Collaboration), Astrophys. J. Lett. **911**, L34 (2021).
[67] S. Chen *et al.* (EPTA Collaboration), Mon. Not. R. Astron. Soc. **508**, 4970 (2021).
[68] B. Goncharov *et al.*, Astrophys. J. Lett. **917**, L19 (2021).
[69] J. Antoniadis *et al.*, Mon. Not. R. Astron. Soc. **510**, 4873 (2022).
[70] A. S. Josan, A. M. Green, and K. A. Malik, Phys. Rev. D **79**, 103520 (2009).
[71] J. Adamek, D. Daverio, R. Durrer, and M. Kunz, J. Cosmol. Astropart. Phys. 07 (2016) 053.